HHS Public Access

Author manuscript

Biol Psychiatry. Author manuscript; available in PMC 2021 May 01.

Published in final edited form as:

Biol Psychiatry. 2020 May 01; 87(9): 829–842. doi:10.1016/j.biopsych.2019.12.025.

Low-dose Perampanel rescues cortical gamma dysregulation associated with parvalbumin interneuron GluA2 upregulation in epileptic Syngap1$^{+/-}$ mice

Brennan J. Sullivan[1], **Simon Ammanuel**[2], **Pavel A. Kipnis**[1], **Yoichi Araki**[3], **Richard L. Huganir**[3], **Shilpa D. Kadam**[1,4,*]

[1]Neuroscience Laboratory, Hugo Moser Research Institute at Kennedy Krieger, Baltimore, MD, 21205, USA

[2]School of Medicine, University of California, San Francisco, 505 Parnassus Avenue, San Francisco, CA, 94143, USA.

[3]Department of Neuroscience, Kavli Neuroscience Discovery Institute, Johns Hopkins University School of Medicine, Baltimore, MD 21205, USA

[4]Department of Neurology, Johns Hopkins University School of Medicine, Baltimore, MD, 21205, USA;

Abstract

BACKGROUND: Loss-of-function *SYNGAP1* mutations cause a neurodevelopmental disorder characterized by intellectual disability and epilepsy. SYNGAP1 is a Ras-GTPase-activating protein that underlies the formation and experience-dependent regulation of postsynaptic densities. The mechanisms that contribute to this proposed monogenic cause of intellectual disability and epilepsy remain unresolved.

METHODS: Here, we establish the phenotype of the epileptogenesis in a *Syngap1*$^{+/-}$ mouse model using 24h video electroencephalogram/electromyogram (vEEG/EMG) recordings at advancing ages. We administered an acute low-dose of Perampanel, an FDA approved AMPAR antagonist, during a follow-on 24h vEEG to investigate the role of AMPARs in *SYNGAP1* haploinsufficiency. To determine the region- and location-specific differences in the expression of the GluA2 AMPAR subunit, immunohistochemistry was performed.

[*]**Corresponding Author:** Shilpa D. Kadam, PhD, Hugo Moser Research Institute at Kennedy Krieger; Department of Neurology, Johns Hopkins University School of Medicine, 707 North Broadway, 400H; Baltimore, MD 21205, Phone: 443-923-2688, Fax: 443-923-2695, kadam@kennedykrieger.org.

Author Contributions

S.D.K. designed the experiments. S.D.K and R.L.H conceptualized the project. S.D.K. and B.J.S performed experiments. Y.A. managed mouse colonies. B.J.S., S.A., and P.A.K. analyzed data. S.D.K. and B.J.S interpreted the data. S.D.K and B.J.S wrote the manuscript. S.D.K., B.J.S., and P.A.K. edited and reviewed the manuscript.

Competing Interests

The authors report no biomedical financial interests or potential conflicts of interest.

RESULTS: A progressive worsening of the epilepsy with emergence of multiple seizure phenotypes, interictal spike frequency, sleep dysfunction, and hyperactivity was identified in *Syngap1*$^{+/-}$ mice. Interictal spikes emerged predominantly during NREM in 24h vEEG of *Syngap1*$^{+/-}$ mice. Myoclonic seizures occurred at behavioral-state transitions both in *Syngap1*$^{+/-}$ mice and during an overnight EEG from a child with *SYNGAP1* haploinsufficiency. In *Syngap1*$^{+/-}$ mice, EEG spectral power analyses identified a significant loss of gamma power modulation during behavioral-state transitions. A significant region-specific increase of GluA2 AMPAR subunit expression in the somas of parvalbumin-positive (PV+) interneurons was identified.

CONCLUSIONS: Acute dosing with Perampanel significantly rescued behavioral-state dependent cortical gamma homeostasis, identifying a novel mechanism implicating Ca^{2+} impermeable AMPARs on PV+ interneurons underlying circuit dysfunction in *SYNGAP1* haploinsufficiency.

Keywords

Myoclonic seizures; gamma oscillations; parvalbumin interneurons; Perampanel; GluA2; intellectual disability

INTRODUCTION

SYNGAP1 codes for synaptic Ras GTPase activating protein 1 (SYNGAP1), a RasGAP critical for the formation of postsynaptic densities (PSDs) and the experience-dependent AMPA receptor (AMPAR) insertion that underlies synaptic plasticity (1–5). Mutations in *SYNGAP1* are prevalent in patients with schizophrenia, intellectual disability (ID), and autism spectrum disorder (6–8). Loss-of-function *SYNGAP1* mutations result in haploinsufficiency and cause mental retardation type 5 (MRD5, OMIM#612621), a severe distinct generalized developmental and epileptic encephalopathy with ID, ataxia, severe behavioral problems, and a risk for autism (6–12).

The majority of patients with MRD5 have refractory epilepsy (12). Poor quality sleep is highly prevalent in patients with neurodevelopmental disorders (NDDs) and epilepsy (13,14). The relationship between epilepsy and sleep is a major focus of ongoing clinical and pre-clinical research (13–15). For example, Rett syndrome (RTT) is an NDD with epilepsy and sleep dysfunction (16,17). Research in both pre-clinical models of RTT and patients with RTT has identified translatable quantitative EEG (qEEG) biomarkers (17,18). There is an urgent need to develop robust biomarkers for NDDs, as bench-to-bedside therapeutic strategies are severely hindered without validated quantitative outcome measures.

Patients with MRD5 predominantly present with myoclonic, absence, or tonic-clonic seizures (8,12). Children with epileptic encephalopathies have a slow developmental regression that is primarily due to seizures, interictal spikes (IISs), or cortical dysrhythmia identified on EEG (19,20). Case reports indicate that adult patients demonstrate gradual decline in cognitive abilities (21). Perampanel (PMP), a recently FDA approved AMPAR antagonist has shown significant promise for multiple seizure types in idiopathic generalized

epilepsies including absence (22). Its use in infants with epilepsy is in clinical trial (23). However, the role of AMPAR antagonists such as PMP in *SYNGAP1* haploinsufficiency related seizures and ID is unknown.

Mice with *Syngap1* haploinsufficiency (*Syngap1*$^{+/-}$) are relevant translational models presenting with learning and memory deficits, abnormal dendritic spine dynamics, cortical hyperexcitability, and precocious unsilencing of thalamocortical synapses during development (24–26). Currently, no studies have investigated the epileptogenesis, sleep, and underlying mechanisms associated with MRD5. An understanding of the mechanisms that promote spontaneous seizures and network dysfunction can help accelerate the discovery of novel therapeutic strategies. For this purpose, a *Syngap1*$^{+/-}$ loss-of-function mouse model (26) (exon 7 and 8 deletions) underwent 24h video-vEEG/EMG recordings at advancing ages (P60-P120). A subsequent 24h EEG investigated the effect of low-dose PMP on EEG-identified biomarkers.

METHODS AND MATERIALS

Animals

All animal care and procedures were carried out in accordance with the recommendations in the Guide for Care and Use of Laboratory Animals of the National Institutes of Health. All protocols used in this study were approved by the Committee on the Ethics of Animals Experiments of the Johns Hopkins University. In *Syngap1*$^{+/-}$ mice, exons 7 and 8 (C2 domain) were replaced with a neomycin resistance gene in the opposite direction to eliminate all possible slice variants (26). All mice were single-housed at P46 (7d before electrode implantation surgeries) in polycarbonate cages with food and water provided *ad libitum*, on a 12h light-dark cycle. All efforts were made to minimize animal suffering and the total number of animals used.

Surgery and 24h Video-EEG/EMG

All surgical procedures implemented in this study are as previously published (27). Briefly, subdural EEG and suprascapular EMG electrode implantation was performed under isoflurane anesthesia (4–1.5%). EEG screw electrodes utilized coordinates from bregma for consistent placement (Supplemental Fig. 1), as previously published (18). After recovering from electrode implantation surgery (7±1 day), mice were placed in a recording chamber with food and water provided *ad libitum*. WT$^{+/+}$ and *Syngap1*$^{+/-}$ mice underwent 24h vEEG/EMG recording at younger (P60; WT$^{+/+}$ N=4 mice and Het$^{+/-}$ N=6 mice) and older (P90–120; WT$^{+/+}$ N=4 mice and Het$^{+/-}$ N=7 mice). For further details of EEG acquisition parameters see Supplementary Methods.

Hypnogram and EEG Power Analysis

EEG data were manually scored for Wake, NREM, and REM states for every 10s epoch by a scorer blinded to genotype and sex. All EEG artifacts identified on EEG underwent video confirmation and were removed from all further analyses. All EEG power analysis protocols used in this study are as previously published (27,28). For further details see Supplementary Methods.

Seizure and IIS Scoring

Spontaneous seizures were identified by manual review of all 24h EEGs by a scorer blinded to genotype and sex. IISs were visually analyzed on raw EEG using conservative parameters obtained from obvious pre- and post-ictal spikes for every 5s EEG epoch. For further details on seizure and ISS scoring parameters see Supplementary Methods.

Analysis of Human EEG recording

Continuous overnight EEGs are being acquired with parent consent under approved IRB protocol (29). The EEG channels F4, C4 and O2 were re-referenced to A1 or A2 and exported in the European Data File (EDF) format, de-identified and assigned an ID number. Each epoch was manually scored as Wake, NREM, or REM, as previously published (17). Seizure scoring was performed separately from sleep scoring. For further details, see Supplementary Methods.

Immunohistochemistry

One week after the final EEG recordings (P127), mice were anesthetized with chloral hydrate (300mg/ml; IP) followed by transcardiac perfusion with ice-cold PBS and fixation with PBS buffered formalin (10%). Brains were subsequently cryoprotected and stored at −80°C before cryosectioning. All coronal sections were cut at 14μm and mounted onto Permafrost™ microscope slides before staining. Fluorescent images were acquired at 10X and 40X using Z-stacks with Axiovision Software 4.6 and Apotome® (Carl Zeiss, Jena, Germany). All data analyses were performed using the ImageJ software (30). All data were analyzed by a scorer blinded to genotype and sex. For further details, see Supplementary Methods.

Statistical Analyses

Statistical tests were performed using Prism 8.3 (GraphPad Software, La Jolla, CA, USA). All 1-way and 2-way ANOVAs were performed with Bonferroni's post-hoc corrections. All independent *t*-tests and *Nested t-tests* were two-tailed. In this study, all data are reported as means ± 1 S.E.M. For further details, see Supplementary Methods.

RESULTS

Syngap1$^{+/-}$ mice have recurrent spontaneous seizures with multiple phenotypes

Continuous 24h vEEG/EMG recordings at temporally advancing ages identified spontaneous seizures in 50% (n/n mice; 4/8) of *Syngap1*$^{+/-}$ mice (Fig. 1). At P60 all seizures were myoclonic (n/n seizures; 5/5); 80% (4/5) of these seizures started in non-rapid eye movement (NREM) at transitions from NREM to wake (Fig. 1A). Myoclonic seizures were 34.4±5.9s in duration with rhythmic spike-wave discharges occurring ~3–4Hz (Fig. 1A), similar to clinical reports (12). The myoclonic seizures were distinguished by their time-locked myoclonic jerks recorded on EMG with video confirmation of head, neck, and upper shoulder myoclonic jerks (see Supplemental Video 1).

Multiple seizure phenotypes were identified in P120$^{+/-}$ mice, consistent with the latest clinical reports (12,31). Myoclonic, generalized tonic-clonic, and electrographic seizures

were observed (Fig. 1B–C and Supplemental Fig. 2). All myoclonic (n/n seizures; 3/11 seizures) and tonic-clonic seizures (1/11) occurred during NREM in $P120^{+/-}$ mice, whereas all electrographic seizures occurred during wake (7/11 seizures; Fig 1C3). Electrographic (subclinical) seizures were distinguished by their abnormal EEG patterns that were apparent only on EEG and not associated with any behavioral change. Myoclonic seizures had a propensity to emerge during NREM regardless of age. From P60 to P120, the average seizure duration significantly increased from 27±0.6 to 106±22.7s (Fig. 1C1). This increase in seizure duration was driven by the emergence of electrographic seizures at P120.

Recurrent generalized seizures in human *SYNGAP1* haploinsufficiency show affinity for transition-states and clustering in NREM.

To evaluate the translational value of 24h qEEG analysis in *Syngap1*$^{+/-}$ mice, two EEG recordings from children diagnosed with *SYNGAP1* haploinsufficiency related epilepsy were acquired (29), and analyzed. A 20h continuous EEG captured an entire cycle of overnight sleep in a 3-year-old boy with *SYNGAP1* haploinsufficiency (Fig. 2). Global seizures were identified as bursts of 3–4Hz spike and slow waves that lasted ~0.5–3s (Fig. 2A). All ictal events observed during sleep occurred in NREM (Fig. 2B), and an affinity for clustering of ictal events (i.e. inter-ictal durations <5min) during NREM was noted (Fig. 2C–D). Further, ictal events predominantly occurred during Wake-NREM and NREM-REM transitions. A 50min clinical EEG recorded from a 5-year-old girl diagnosed with *SYNGAP1* haploinsufficiency showed a similar clustering of generalized ~3–4Hz short-duration seizures during transitions from Wake to first NREM (Supplemental Fig. 3). These observations identified a previously undescribed clustering of ictal-events during NREM, and the propensity of the ictal clusters to occur during transitions between behavioral-states.

Progressive alterations in macro-sleep architecture

Sleep dysfunction is a common feature of NDDs and is reported in patients with *SYNGAP1* haploinsufficiency (12,21). Quantitative assessments of the sleep problems in patients with *SYNGAP1* haploinsufficiency are lacking, therefore future assessments will be informative (29). In this study, the $WT^{+/+}$ macro-sleep architecture was ultradian with 15.38±2.2 sleep cycles occurring over 24h (Fig. 3A). All $WT^{+/+}$ mice regardless of age demonstrated a consistent sleep architecture (Supplemental Fig. 4). $WT^{+/+}$ mice spent ~80% of the time awake during the dark phase (Fig. 3A–B2), demonstrating the nocturnal predominance of activity in $WT^{+/+}$ mice. Between groups, $P60^{+/-}$ and $P120^{+/-}$ mice spent more time asleep than $WT^{+/+}$ mice over 24h (Fig. 3B). Compared to $WT^{+/+}$ mice, $P120^{+/-}$ mice spent significantly more time asleep during the light phase (Fig. 3B1). In $WT^{+/+}$ mice, there were significantly fewer sleep/wake cycles during the dark phase (10.37±2.0 cycles) compared to the light phase (22.13±3.3 cycles, Fig. 3C). In $P60^{+/-}$ and $P120^{+/-}$ mice, the difference between the numbers of sleep/wake cycles during light vs. dark phase was not significant (Fig. 3C). In contrast to the significant differences in macro-sleep architecture, all mice maintained a sleep microarchitecture of ~80% NREM and ~ 20% REM during the 24h recordings (Fig. 3C1–C2).

IISs predominantly occurred during NREM sleep and were progressive with age.

Uncontrolled epilepsy is at least partially responsible for cognitive regression in children with epileptic encephalopathies (19,20). All *Syngap1*$^{+/-}$ mice presented IISs during both sleep and wake (Fig. 4A–B). IIS frequency significantly increased at P120$^{+/-}$ when compared to WT$^{+/+}$ mice (1-way ANOVA, $F_{2,20}$=4.278, p=0.0284). This significant increase was driven by IISs that occurred during NREM sleep, specifically during light-phase sleep (Fig. 4C–D). Furthermore, even though the total duration of sleep increased significantly in P120$^{+/-}$ mice, (Fig. 3B) the rate of IIS occurrence per hour of NREM sleep was significantly greater in P120$^{+/-}$ mice compared to WT$^{+/+}$ (Fig. 4D).

Emerging research utilizing intracranial recordings from epilepsy patients has demonstrated that regulation of brain activity occurs on long timescales(32). Daily patterns of seizure occurrence demonstrate circadian rhythmicity and clustering organization(32). In this study, we report the relationship between seizure occurrence and frequency distribution of IISs over 24h for all mice (Fig. 4E–F). Grouped data of IIS frequency averaged over 24h showed an escalation in IIS frequency at the beginning of the light phase, and was associated with an increased incidence of seizures in P120$^{+/-}$ mice. Antagonizing AMPARs acutely with PMP (2mg/kg I.P. at 10AM and 6PM) prevented seizures during the 24h EEG, but did not significantly reduce IIS frequency (Supplemental Fig. 5). In summary, IIS occurrence was greatest during NREM in *Syngap1*$^{+/-}$ mice.

Hyperactivity worsened with age

Video tracking software allows for high specificity and sensitivity when tracking mouse motor activity over the 24h recordings. Total distance traveled by each mouse over a 24h period was used to identify hyperactivity in *Syngap1*$^{+/-}$ mice (Fig. 5A1–A3). Compared to WT$^{+/+}$ mice (267.92±46.8m), P120$^{+/-}$ mice traveled greater distances (479.75±46.1m), which was not detected in the P60$^{+/-}$ mice (288.22±32m; Fig. 5A2–A3). Since P120$^{+/-}$ mice spent more time asleep than WT$^{+/+}$ mice (Fig. 3), the distance traveled by each mouse was normalized to the duration of time spent asleep. The running average of mice in each group highlighted increased activity at the end of the dark phase, when the majority of nesting behavior occurs (33) (Fig. 5B). The normalized distance traveled by P120$^{+/-}$ mice was significantly greater than WT$^{+/+}$ and P60$^{+/-}$ mice (Fig. 5C). P120$^{+/-}$ mice spent more time asleep, but were hyperactive when awake, as they travelled twice the distance compared to WT$^{+/+}$ mice. These results are consistent with recent reports of home cage hyperactivity in male *Syngap1*$^{+/-}$ mice (34,35).

Activity-dependent theta modulation is impaired during wake in P120$^{+/-}$

Cross–frequency coupling occurs between theta and gamma oscillations(36,37). Specifically, gamma oscillations are nested within theta oscillations(38,39) and are critical for memory retrieval (40–42). To determine differences in theta and gamma power during transitions from stationary- to active-wake, 10min epochs were analyzed (Fig. 6A). During stationary-wake, high theta and low gamma power were apparent in WT$^{+/+}$ mice (Fig. 6A–B). After the transition to active-wake, WT$^{+/+}$ mice had high gamma and low theta power. The state-dependent (stationary- vs. active-wake) modulation of theta power was not apparent in P120$^{+/-}$ mice (Fig. 6B–C).

In $WT^{+/+}$ mice, theta and gamma spectral power demonstrated an inverse relationship during wake-sleep state transitions (Supplemental Fig. 6A). During wake, the theta-gamma ratio (TGR) was low in $WT^{+/+}$ mice, while during sleep the TGR was high (Supplemental Fig. 6A) (43,44). This relationship between theta and gamma power was lost in $P120^{+/-}$ mice (Supplemental Fig.6A–B).

Loss of behavioral-state homeostasis of cortical gamma

High cognitive load during wakefulness (45–47) is associated with increased gamma power. Accordingly, in $WT^{+/+}$ mice gamma power was high during wake and low during NREM sleep (Fig. 7A). $P120^{+/-}$ mice did not demonstrate this behavioral state-dependent gamma power modulation during Wake-NREM transitions, as gamma power remained high during NREM (Fig. 7B). PMP-treated *Syngap1*$^{+/-}$ mice showed a significant rescue of the gamma dysregulation, high gamma during wake, and low gamma during NREM similar to $WT^{+/+}$ mice (Fig. 7C). In $WT^{+/+}$ mice the slopes of gamma power during Wake-NREM transitions over 24h were negative, as gamma power decreased during NREM. During NREM-Wake transitions, the slope of gamma power was positive in $WT^{+/+}$ mice as gamma power increased during wake (Fig. 7D1). These negative slopes of Wake-NREM transitions and the positive slopes of NREM-Wake transitions were significantly different from one another in $WT^{+/+}$ mice (Fig. 7D1). $P120^{+/-}$ mice failed to show significant differences between gamma slopes (Fig. 7D2). PMP significantly rescued the transition state-dependent differences between the slopes of gamma power in the *Syngap1*$^{+/-}$ mice (Fig. 7D3). The average gamma slopes for both Wake-NREM and NREM-Wake transitions were compared between groups (Supplemental Fig. 7). Mean gamma slopes between NREM-Wake and Wake-NREM transitions in $WT^{+/+}$ mice were significantly different, and were lost in $P120^{+/-}$ mice. PMP rescued this loss in the $P120^{+/-}$ mice (Supplemental Fig. 7). Further, low-dose PMP did not significantly alter cortical gamma during transitions between Wake and Sleep in the $WT^{+/+}$ mice that were administered PMP (Supplemental Fig. 8).

Additional analyses of binned gamma power were undertaken as spectral frequency analysis identified that the significant behavioral-state alterations in $P120^{+/-}$ gamma power modulation between NREM and Wake were predominantly driven within the 35–45Hz range (Supplemental Fig. 9). Power in the 35–45Hz bin was significantly higher during Wake compared to NREM in $WT^{+/+}$ mice (Supplemental Fig. 9), which was lost and reversed in $P120^{+/-}$ mice (Supplemental Fig. 9). In summary, *Syngap1*$^{+/-}$ mice showed a loss of state-dependent gamma modulation.

During NREM the majority of brain activity is synchronous slow wave activity with low gamma power (45–47). In contrast, gamma power increases during the asynchronous activity of REM (45–47), hence its description as *paradoxical sleep*. In $WT^{+/+}$ mice, NREM-REM transitions underwent modulation in gamma, theta, and delta powers (Fig. 8A & B). A significantly lower percent change in gamma power during NREM-REM transitions was apparent in $P120^{+/-}$ mice compared to $WT^{+/+}$. This impairment in gamma power modulation from NREM to REM was significantly rescued by PMP (Fig. 8B).

Deficits in PV+IN innervation in prefrontal cortex

The majority of perisomatic inhibition is mediated by parvalbumin-positive interneurons (PV+INs) (45), which have a significant role in the modulation of cortical gamma oscillations(48). Our novel finding of consistently high gamma power in *Syngap1*$^{+/-}$ mice directed the investigation of PV+IN density distribution in the cerebral cortex, hippocampus, and prefrontal cortices. PV+IN distributions did not show significant differences in overall densities in the either the dorsal pallidum cortex (DP; WT$^{+/+}$ vs. Het$^{+/-}$: *Nested t-test,* t_{14}=0.6823, p=0.51*)* or the prelimbic cortex (PrL; WT$^{+/+}$ vs. Het$^{+/-}$: *Nested t-test,* t_{14}=0.5755, p=0.46*)*. The quantification of total and perisomatic PV+ puncta counts identified significant deficits in the DP cortex of *Syngap1*$^{+/-}$ mice (Fig. 9A–B), but not in the PrL cortex (PrL Total PV counts WT$^{+/+}$ vs. Het$^{+/-}$: *Nested t-test* t_{14}=0.055, p=0.95 and PrL Soma PV counts WT$^{+/+}$ vs. Het$^{+/}$: t_{14}=1.434, p=0.1734). GluA2 fluorescence intensity on PV+IN somas (putative Ca^{2}+ impermeable AMPARs) and non-PV+ neurons showed no significant differences in DP (Fig. 9C–D; for antibody verification see Supplemental Fig. 10), or PrL. These findings indicate that deficits in PV+IN innervation were region-specific within the prefrontal cortex in *Syngap1*$^{+/-}$ mice.

These findings warranted the analysis of PV+ puncta counts in other ROIs. Unlike the prefrontal cortex, no significant differences in PV+ puncta count were noted in either the barrel (BCX) or motor (MCX; Fig. 10A1) cortices. A layer-specific investigation of BCX and MCX demonstrated that PV+ puncta counts were not significantly different between layers for both the total counts, and the non-PV+ somas (Fig. 10A1–B1). In the hippocampus, PV+ puncta counts were not significantly different in CA1 or CA3 (Fig. 10C1). Normalized PV+ puncta counts were not significantly different between the SP, SR, or SO of WT$^{+/+}$ and P120$^{+/-}$ mice in CA1 and CA3. In summary, deficits in PV+ innervation were only observed in the DP cortex.

Increased GluA2 expression on PV+ soma in somatosensory but not motor cortex

A rich diversity of GABAergic neurons shape the spatiotemporal dynamics of cortical circuit outputs by elegant inhibitory control mechanisms(49,50). Previous research reports that compared to pyramidal neurons, PV+INs have a lower expression profile for the GluA2 subunit(51). PV+INs in the both L2–3 and L5–6 of the BCX showed significant upregulation of GluA2 (Fig. 10A2), which was absent in the MCX (Fig. 10B2). The mean GluA2 fluorescence intensity on PV+INs was also significantly higher in the CA3 but not in the CA1 (Fig. 10C2). No significant differences in GluA2 fluorescence intensities were noted in the non-PV+ cells in any ROI investigated (Supplemental Fig. 11). Since all *Syngap1*$^{+/-}$ mice were epileptic, the hippocampi were investigated for mossy fiber sprouting. No evidence for mossy fiber sprouting was detected in this model (Supplemental Fig. 12). In summary, a significant region-specific upregulation of GluA2 expression in PV +INs, a population of INs known to generate cortical gamma oscillations (48), was detected in *Syngap1*$^{+/-}$ mice.

DISCUSSION

24h continuous EEG monitoring and qEEG protocols (27) identified novel biomarkers underlying epileptogenesis in a mouse model of *Syngap1* haploinsufficiency. A progressive worsening in epileptogenesis, IIS frequency, hyperactivity, and an impaired behavioral-state dependent modulation of cortical gamma activity during both Wake- and Sleep-state transitions was identified. Myoclonic ~3Hz seizures in the *Syngap1*$^{+/-}$ mice arose during NREM sleep. Human overnight and clinical EEG analyses identified ictal clusters of 3Hz spike-wave discharges during NREM that were aggravated at transitions from Wake to Sleep and Sleep to Wake. Currently, it is unknown if any other models of *Syngap1* haploinsufficiency that differ by mutation site or mutation strategy (i.e. germ-line vs. Cre-recombinase) show these clinically relevant 3Hz seizures with progression to multiple other phenotypes. Additionally, the rescue of impaired cortical gamma homeostasis during behavioral-state transitions by PMP identified the critical role of AMPARs in during such transitions. Induced increase of GluA2 expression in INs resulted in severe disruption of gamma oscillations (52). This research implicated the Ca^{2}+ impermeable AMPAR subunit, which confers a slow EPSP in excitatory neurons, and usually expressed at low levels in GABAergic interneurons (52), in playing a critical role in gamma power during behavioral-state transitions. Immuno-labelling identified excessive GluA2-AMPAR expression on the somas of PV+INs in *Syngap1*$^{+/-}$ mice that was location-specific, supporting our hypothesis.

In this study, 50% of the *Syngap1*$^{+/-}$ mice presenting with seizures during the 24 recording period indicating a high incidence of seizures. Progressive worsening of the sleep dysfunction and increasing NREM IIS frequency in 100% of the mice is also a common feature of several developmental disorders associated with epilepsy (53–59).

Wakefulness is associated with net-synaptic potentiation, whereas sleep favors global synaptic depression thereby preserving an overall balance of synaptic strength (60). AMPAR levels are high during wakefulness and low during sleep. The global reduction of AMPARs during sleep may be disrupted in *Syngap1*$^{+/-}$ mice as haploinsufficiency could result in the inability to regulate Ras and Rap, two proteins that are involved in the regulation of surface AMPARs (3,4,61–64). The inability to downregulate surface AMPARs during transition-state synaptic homeostasis could lead to chronic overexpression of AMPARs in highly active neurons, such as fast spiking PV+INs.

The significant loss in cortical gamma homeostasis associated with behavioral-state transitions in *Syngap1*$^{+/-}$ mice could critically impede cortical information processing. Gamma oscillations (52,65) are known to depend upon AMPAR kinetics in interneurons, especially for long-range synchrony. The significant rescue of the cortical gamma homeostasis by acute dosing of low-dose PMP when compared to the relatively weaker effect on IIS suppression may indicate a novel role for PMP beyond its FDA approved anti-seizure properties. New trials evaluating PMP efficacy in infants (23) are underway. In the clinic, PMP dosing is gradually ramped-up starting with the low-dose of 2mg/kg in weekly increments reaching maintenance doses of 8–12 mg/day based on tolerability. The acute low-dose protocol used here did not show significant effects on IIS suppression; however no seizure events were noted with PMP treatment. PMP anti-seizure efficacy for SYNGAP1-

related seizures are currently unknown, and a recent cohort study with 57 patients reported only one patient having received PMP treatment (12). The findings indicate the necessity to develop GluA2-AMPAR selective antagonists, which currently do not exist. These analyses also identified poor PV+IN innervation in the prefrontal cortex supported by previously published reports(66), and was not detected in the other ROIs.

Increasingly, brain oscillations are being used to understand complex neuropsychiatric disorders. Gamma (35–50Hz) oscillations have warranted special attention due to their association with higher order cognitive processes including sensory processing, attention, working memory, and executive functioning. Activation of GABAergic interneuron networks has been shown to produce gamma oscillations (~40Hz) in both the hippocampal and neocortical networks. Given the critical role of PV+INs in cortical gamma oscillations (48,67) and the role of AMPARs in homeostatic synaptic plasticity (68), the loss of gamma homeostasis identified for *Syngap1* haploinsufficiency during periods commonly associated with intense synaptic plasticity (69) provide novel insights into the associated intellectual disabilities. AMPA-mediated currents rise and decay faster in interneurons partly because of these differences in subunit profiles (70,71). PV+INs receive convergent excitatory input from principal neurons, and inhibitory input primarily from other PV+INs. Experiments that have causally tested stimulation of PV+ cells *in vivo* in the BCX by ontogenetic manipulation selectively amplified gamma oscillations (72). Importantly, this activation suppressed the sensory processing in nearby excitatory neurons within the BCX. Findings of increased GluA2 AMPARs on PV+ soma both in layers 2/3 and 5/6 of the BCX would predict similar suppression of sensory processing in the BCX (73). An increase of GluA2 expression in PV+INs in the BCX could implicate recruitment of excessive PV+IN mediated inhibition resulting in cortical hyperexcitability via rebound excitation. This hypothesis may underlie the clinical reports of reflex seizures in MRD5 emerging during activities associated with increased cortical gamma synchronicity (12,31), a role in which electrically-coupled projection PV+IN are significantly involved.

Morphology of PV+INs has been identified as unipolar vs. multipolar (74) and little is known about the differences in AMPA-mediated currents in these subtypes. GluA2-lacking AMPARs promote anti-Hebbian long-term plasticity (75) which is critical for projection interneurons that functionally connect spatially distant circuits during development. Increase of GluA2-AMPARs in PV+IN soma could be one novel mechanism underlying autistic-like behaviors, ID, and seizures in *SYNGAP1* haploinsufficiency. Little is known of the developmental and regional expression profiles of SYNGAP1 isoforms, however it is known that they can exert opposing effects on synaptic strength (76).

To summarize, SYNGAP1 regulates synaptic plasticity, and this process is heavily involved in both epileptogenesis and sleep homeostasis. Investigation of circuit function in intact brains using qEEG biomarkers as they transition from active exploratory, inactive-Wake, and REM/NREM sleep states is an exciting frontier. These behavioral-state transitions are the most reliant upon synaptic plasticity.

Supplementary Material

Refer to Web version on PubMed Central for supplementary material.

ACKNOWLEDGEMENTS AND DISCLOSURES

We thank the families who have consented to participate in the post-hoc analyses of overnight EEGs recorded in their children with identified pathogenic *SYNGAP1* mutations. The authors would like to thank the Bridge the Gap SYNGAP foundation for help with patient EEG acquisition. The authors would like to thank Dr. Jonathan Pevsner for his thoughtful comments and suggestions and Dr. Inge Hong for his help with the GluA2 KO immunohistochemistry experiments. Research reported in this publication was supported by the Eunice Kennedy Shriver National Institute of Child Health and Human Development of the National Institutes of Health under Award Number R01HD090884 (SDK). The content is solely the responsibility of the authors and does not necessarily represent the official views of the National Institutes of Health. This manuscript was previously uploaded as a preprint to bioRxiv (doi: https://doi.org/10.1101/718965).

Abbreviations list:

AMPAR	AMPA receptor
PV+IN	parvalbumin interneuron
IIS	interictal spike
BCX	barrel cortex
MCX	motor cortex
PMP	Perampanel
CA1	cornu Ammonis 1
CA3	cornu Ammonis 3
Sr	stratum radiatum
SO	stratum oriens
SP	stratum pyramidale
DP	dorsal pallidum
PrL	prelimbic cortex
MRD5	mental retardation type 5
PSD	postsynaptic density
NREM	non-rapid eye movement
REM	rapid eye movement
EEG	electroencephalogram
EMG	electromyogram
NDD	neurodevelopmental disorder

TGR	theta-gamma ratio
IHC	immunohistochemical
FFT	fast Fourier transform

References

1. Chen H-J, Rojas-Soto M, Oguni A, Kennedy MB (1998): A Synaptic Ras-GTPase Activating Protein (p135 SynGAP) Inhibited by CaM Kinase II. Neuron 20: 895–904. [PubMed: 9620694]
2. Kim JH, Liao D, Lau LF, Huganir RL (1998): SynGAP: a synaptic RasGAP that associates with the PSD-95/SAP90 protein family. Neuron 20: 683–691. [PubMed: 9581761]
3. Rumbaugh G, Adams JP, Kim JH, Huganir RL (2006): SynGAP regulates synaptic strength and mitogen-activated protein kinases in cultured neurons. Proc Natl Acad Sci U S A 103: 4344–4351. [PubMed: 16537406]
4. Araki Y, Zeng M, Zhang M, Huganir RL (2015): Rapid dispersion of SynGAP from synaptic spines triggers AMPA receptor insertion and spine enlargement during LTP., Rapid Dispersion of SynGAP from Synaptic Spines Triggers AMPA Receptor Insertion and Spine Enlargement during LTP. Neuron Neuron 85, 85: 173, 173–189. [PubMed: 25569349]
5. Zeng M, Bai G, Zhang M (2017): Anchoring high concentrations of SynGAP at postsynaptic densities via liquid-liquid phase separation. Small GTPases 1–9.
6. Purcell SM, Moran JL, Fromer M, Ruderfer D, Solovieff N, Roussos P, et al. (2014): A polygenic burden of rare disruptive mutations in schizophrenia. Nature 506: 185–190. [PubMed: 24463508]
7. Hamdan FF, Gauthier J, Spiegelman D, Noreau A, Yang Y, Pellerin S, et al. (2009): Mutations in SYNGAP1 in autosomal nonsyndromic mental retardation. N Engl J Med 360: 599–605. [PubMed: 19196676]
8. Hamdan FF, Daoud H, Piton A, Gauthier J, Dobrzeniecka S, Krebs M-O, et al. (2011): De novo SYNGAP1 mutations in nonsyndromic intellectual disability and autism. Biol Psychiatry 69: 898–901. [PubMed: 21237447]
9. Berryer Martin H, Hamdan Fadi F, Klitten Laura L, Møller Rikke S, Carmant Lionel, Schwartzentruber Jeremy, et al. (2012): Mutations in SYNGAP1 Cause Intellectual Disability, Autism, and a Specific Form of Epilepsy by Inducing Haploinsufficiency. Hum Mutat 34: 385–394. [PubMed: 23161826]
10. Carvill GL, Heavin SB, Yendle SC, McMahon JM, O'Roak BJ, Cook J, et al. (2013): Targeted resequencing in epileptic encephalopathies identifies *de novo* mutations in *CHD2* and *SYNGAP1*. Nat Genet 45: 825–830. [PubMed: 23708187]
11. Mignot C, Stulpnagel C von, Nava C, Ville D, Sanlaville D, Lesca G, et al. (2016): Genetic and neurodevelopmental spectrum of SYNGAP1-associated intellectual disability and epilepsy. J Med Genet 53: 511–522. [PubMed: 26989088]
12. Vlaskamp DRM, Shaw BJ, Burgess R, Mei D, Montomoli M, Xie H, et al. (2019): SYNGAP1 encephalopathy: A distinctive generalized developmental and epileptic encephalopathy. Neurology 92: e96–e107. [PubMed: 30541864]
13. Jain SV, Kothare SV (2015): Sleep and Epilepsy. Semin Pediatr Neurol 22: 86–92. [PubMed: 26072338]
14. Robinson-Shelton A, Malow BA (2015): Sleep Disturbances in Neurodevelopmental Disorders. Curr Psychiatry Rep 18: 6.
15. Malow BA (2004): Sleep disorders, epilepsy, and autism. Ment Retard Dev Disabil Res Rev 10: 122–125. [PubMed: 15362168]
16. Glaze DG (2005): Neurophysiology of Rett syndrome. J Child Neurol 20: 740–746. [PubMed: 16225829]
17. Ammanuel S, Chan WC, Adler DA, Lakshamanan BM, Gupta SS, Ewen JB, et al. (2015): Heightened Delta Power during Slow-Wave-Sleep in Patients with Rett Syndrome Associated with Poor Sleep Efficiency. PLoS One 10: e0138113–. [PubMed: 26444000]

18. Johnston MV, Ammanuel S, O'Driscoll C, Wozniak A, Naidu S, Kadam SD (2014): Twenty-four hour quantitative-EEG and in-vivo glutamate biosensor detects activity and circadian rhythm dependent biomarkers of pathogenesis in Mecp2 null mice. Front SystNeurosci 8: 118–.
19. Holmes GL (2005): Effects of seizures on brain development: lessons from the laboratory. Pediatr Neurol 33: 1–11. [PubMed: 15993318]
20. Nabbout R, Dulac O (2003): Epileptic encephalopathies: a brief overview. J Clin Neurophysiol Off Publ Am Electroencephalogr Soc 20: 393–397.
21. Prchalova D, Havlovicova M, Sterbova K, Stranecky V, Hancarova M, Sedlacek Z (2017): Analysis of 31-year-old patient with SYNGAP1 gene defect points to importance of variants in broader splice regions and reveals developmental trajectory of SYNGAP1-associated phenotype: case report. BMC Med Genet 18 10.1186/s12881-017-0425-4
22. Villanueva V, Montoya J, Castillo A, Mauri-Llerda JÁ, Giner P, López-González FJ, et al. (2018): Perampanel in routine clinical use in idiopathic generalized epilepsy: The 12-month GENERAL study. Epilepsia 59: 1740–1752. [PubMed: 30062784]
23. Clinical Trial (n.d.): Perampanel Study for Infants with Epilepsy. Epilepsy Foundation. Retrieved January 23, 2019, from https://www.epilepsy.com/clinical_trials/perampanel-study-infants-epilepsy
24. Clement JP, Ozkan ED, Aceti M, Miller CA, Rumbaugh G (2013): SYNGAP1 Links the Maturation Rate of Excitatory Synapses to the Duration of Critical-Period Synaptic Plasticity. J Neurosci 33: 10447–10452. [PubMed: 23785156]
25. Clement JP, Aceti M, Creson TK, Ozkan ED, Shi Y, Reish NJ, et al. (2012): Pathogenic SYNGAP1 mutations impair cognitive development by disrupting maturation of dendritic spine synapses. Cell 151: 709–723. [PubMed: 23141534]
26. Kim JH, Lee H-K, Takamiya K, Huganir RL (2003): The role of synaptic GTPase-activating protein in neuronal development and synaptic plasticity. J Neurosci Off J Soc Neurosci 23: 1119–1124.
27. Kang SK, Ammanuel S, Thodupunuri S, Adler DA, Johnston MV, Kadam SD (2018): Sleep dysfunction following neonatal ischemic seizures are differential by neonatal age of insult as determined by qEEG in a mouse model. Neurobiol Dis 116: 1–12. [PubMed: 29684437]
28. Adler DA, Ammanuel S, Lei J, Dada T, Borbiev T, Johnston MV, et al. (2014): Circadian cycle-dependent EEG biomarkers of pathogenicity in adult mice following prenatal exposure to in utero inflammation. Neuroscience.
29. SYNGAP1 Research (n.d.): Retrieved July 1, 2019, from https://www.kennedykrieger.org/research/participate-in-research
30. ImageJ Plugins (n.d.): ImageJ. Retrieved July 1, 2019, from https://imagej.nih.gov/ij/plugins/index.html
31. Striano P, Huppke P (2018): A synaptic protein defect associated with reflex seizure disorder. Neurology 10.1212/WNL.0000000000006720.
32. Baud MO, Kleen JK, Mirro EA, Andrechak JC, King-Stephens D, Chang EF, Rao VR (2018): Multi-day rhythms modulate seizure risk in epilepsy. Nat Commun 9: 88. [PubMed: 29311566]
33. Bains RS, Wells S, Sillito RR, Armstrong JD, Cater HL, Banks G, Nolan PM (2018): Assessing mouse behaviour throughout the light/dark cycle using automated in-cage analysis tools. J Neurosci Methods 300: 37–47. [PubMed: 28456660]
34. Nakajima R, Takao K, Hattori S, Shoji H, Komiyama NH, Grant SGN, Miyakawa T (2019): Comprehensive behavioral analysis of heterozygous Syngap1 knockout mice. Neuropsychopharmacol Rep 10.1002/npr2.12073
35. Komiyama NH, Watabe AM, Carlisle HJ, Porter K, Charlesworth P, Monti J, et al. (2002): SynGAP Regulates ERK/MAPK Signaling, Synaptic Plasticity, and Learning in the Complex with Postsynaptic Density 95 and NMDA Receptor. J Neurosci 22: 9721–9732. [PubMed: 12427827]
36. Belluscio MA, Mizuseki K, Schmidt R, Kempter R, Buzsáki G (2012): Cross-frequency phase-phase coupling between θ and γ oscillations in the hippocampus. J Neurosci Off J Soc Neurosci 32: 423–435.
37. Buzsáki G, Anastassiou CA, Koch C (2012): The origin of extracellular fields and currents — EEG, ECoG, LFP and spikes. Nat Rev Neurosci 13: 407–420. [PubMed: 22595786]

38. Bragin A, Jandó G, Nádasdy Z, Hetke J, Wise K, Buzsáki G (1995): Gamma (40–100 Hz) oscillation in the hippocampus of the behaving rat. J Neurosci Off J Soc Neurosci 15: 47–60.
39. Soltesz I, Deschênes M (1993): Low- and high-frequency membrane potential oscillations during theta activity in CA1 and CA3 pyramidal neurons of the rat hippocampus under ketamine-xylazine anesthesia. J Neurophysiol 70: 97–116. [PubMed: 8395591]
40. Axmacher N, Henseler MM, Jensen O, Weinreich I, Elger CE, Fell J (2010): Cross-frequency coupling supports multi-item working memory in the human hippocampus. Proc Natl Acad Sci 107: 3228–3233. [PubMed: 20133762]
41. Demiralp T, Bayraktaroglu Z, Lenz D, Junge S, Busch NA, Maess B, et al. (2007): Gamma amplitudes are coupled to theta phase in human EEG during visual perception. Int J Psychophysiol Off J Int Organ Psychophysiol 64: 24–30.
42. Köster M, Friese U, Schöne B, Trujillo-Barreto N, Gruber T (2014): Theta-gamma coupling during episodic retrieval in the human EEG. Brain Res 1577: 57–68. [PubMed: 24978601]
43. Lisman JE, Jensen O (2013): The Theta-Gamma Neural Code. Neuron 77: 1002–1016. [PubMed: 23522038]
44. Moretti DV, Fracassi C, Pievani M, Geroldi C, Binetti G, Zanetti O, et al. (2009): Increase of theta/gamma ratio is associated with memory impairment. Clin Neurophysiol 120: 295–303. [PubMed: 19121602]
45. Buzsaki G, Wang XJ (2012): Mechanisms of gamma oscillations. Annu Neurosci 35: 203–225.
46. Valderrama M, Crépon B, Botella-Soler V, Martinerie J, Hasboun D, Alvarado-Rojas C, et al. (2012): Human Gamma Oscillations during Slow Wave Sleep. PLoS ONE 7 10.1371/journal.pone.0033477
47. Scheffzük C, Kukushka VI, Vyssotski AL, Draguhn A, Tort ABL, Brankačk J (2011): Selective coupling between theta phase and neocortical fast gamma oscillations during REM-sleep in mice. PloS One 6: e28489. [PubMed: 22163023]
48. Sohal VS, Zhang F, Yizhar O, Deisseroth K (2009): Parvalbumin neurons and gamma rhythms enhance cortical circuit performance. Nature 459: 698–702. [PubMed: 19396159]
49. Tremblay R, Lee S, Rudy B (2016): GABAergic Interneurons in the Neocortex: From Cellular Properties to Circuits. Neuron 91: 260–292. [PubMed: 27477017]
50. Huang ZJ, Paul A (2019): The diversity of GABAergic neurons and neural communication elements. Nat Rev Neurosci 1.
51. Akgül G, McBain CJ (2016): Diverse roles for ionotropic glutamate receptors on inhibitory interneurons in developing and adult brain. J Physiol 594: 5471–5490. [PubMed: 26918438]
52. Fuchs EC, Doheny H, Faulkner H, Caputi A, Traub RD, Bibbig A, et al. (2001): Genetically altered AMPA-type glutamate receptor kinetics in interneurons disrupt long-range synchrony of gamma oscillation. Proc Natl Acad Sci U S A 98: 3571–3576. [PubMed: 11248119]
53. Xu L, Guo D, Liu Y-Y, Qiao D-D, Ye J-Y, Xue R (2018): Juvenile myoclonic epilepsy and sleep. Epilepsy Behav EB 80: 326–330.
54. Gruber R, Wise MS (2016): Sleep Spindle Characteristics in Children with Neurodevelopmental Disorders and Their Relation to Cognition. Neural Plast 2016 10.1155/2016/4724792
55. Singhal NS, Sullivan JE (2014): Continuous Spike-Wave during Slow Wave Sleep and Related Conditions. ISRN Neurol 2014 10.1155/2014/619079
56. Al Keilani MAH, Carlier S, Groswasser J, Dan B, Deconinck N (2011): Rett syndrome associated with continuous spikes and waves during sleep. Acta Neurol Belg 111: 328–332. [PubMed: 22368975]
57. Creson TK, Rojas C, Hwaun E, Vaissiere T, Kilinc M, Jimenez-Gomez A, et al. (2019): Reexpression of SynGAP protein in adulthood improves translatable measures of brain function and behavior ((Westbrook GL, editor)). eLife 8: e46752. [PubMed: 31025938]
58. Ozkan ED, Creson TK, Kramár EA, Rojas C, Seese RR, Babyan AH, et al. (2014): Reduced cognition in Syngap1 mutants is caused by isolated damage within developing forebrain excitatory neurons. Neuron 82: 1317–1333. [PubMed: 24945774]
59. Ujma PP, Simor P, Ferri R, Fabó D, Kelemen A, Erőss L, et al. (2015): Increased interictal spike activity associated with transient slow wave trains during non-rapid eye movement sleep: Increased IEDs in transient SW trains. Sleep Biol Rhythms 13: 155–162.

60. Vyazovskiy VV, Cirelli C, Pfister-Genskow M, Faraguna U, Tononi G (2008): Molecular and electrophysiological evidence for net synaptic potentiation in wake and depression in sleep. Nat Neurosci 11: 200–208. [PubMed: 18204445]
61. Zhu JJ, Qin Y, Zhao M, Van Aelst L, Malinow R (2002): Ras and Rap control AMPA receptor trafficking during synaptic plasticity. Cell 110: 443–455. [PubMed: 12202034]
62. Walkup WG, Washburn L, Sweredoski MJ, Carlisle HJ, Graham RL, Hess S, Kennedy MB (2015): Phosphorylation of synaptic GTPase-activating protein (synGAP) by Ca2+/calmodulin-dependent protein kinase II (CaMKII) and cyclin-dependent kinase 5 (CDK5) alters the ratio of its GAP activity toward Ras and Rap GTPases. J Biol Chem 290: 4908–4927. [PubMed: 25533468]
63. Krapivinsky G, Medina I, Krapivinsky L, Gapon S, Clapham DE (2004): SynGAP-MUPP1-CaMKII Synaptic Complexes Regulate p38 MAP Kinase Activity and NMDA Receptor-Dependent Synaptic AMPA Receptor Potentiation. Neuron 43: 563–574. [PubMed: 15312654]
64. Pena V, Hothorn M, Eberth A, Kaschau N, Parret A, Gremer L, et al. (2008): The C2 domain of SynGAP is essential for stimulation of the Rap GTPase reaction. EMBO Rep 9: 350–355. [PubMed: 18323856]
65. Fuchs EC, Zivkovic AR, Cunningham MO, Middleton S, LeBeau FEN, Bannerman DM, et al. (2007): Recruitment of Parvalbumin-Positive Interneurons Determines Hippocampal Function and Associated Behavior. Neuron 53: 591–604. [PubMed: 17296559]
66. Berryer MH, Chattopadhyaya B, Xing P, Riebe I, Bosoi C, Sanon N, et al. (2016): Decrease of SYNGAP1 in GABAergic cells impairs inhibitory synapse connectivity, synaptic inhibition and cognitive function. Nat Commun 7: 13340. [PubMed: 27827368]
67. Le Magueresse C, Monyer H (2013): GABAergic Interneurons Shape the Functional Maturation of the Cortex. Neuron 77: 388–405. [PubMed: 23395369]
68. Altimimi HF, Stellwagen D (2013): Persistent Synaptic Scaling Independent of AMPA Receptor Subunit Composition. J Neurosci 33: 11763–11767. [PubMed: 23864664]
69. Turrigiano G (2011): Too Many Cooks? Intrinsic and Synaptic Homeostatic Mechanisms in Cortical Circuit Refinement. Annu Rev Neurosci 34: 89–103. [PubMed: 21438687]
70. Jonas P (1994): Differences in Ca2+ permeability of AMPA-type glutamate receptor channels in neocortical neurons caused by differential GluR-B subunit expression. Neuron 12: 1281–1289. [PubMed: 8011338]
71. Hu H, Gan J, Jonas P (2014): Fast-spiking, parvalbumin+ GABAergic interneurons: From cellular design to microcircuit function. Science 345: 1255263–1255263. [PubMed: 25082707]
72. Cardin JA, Carlén M, Meletis K, Knoblich U, Zhang F, Deisseroth K, et al. (2009): Driving fast-spiking cells induces gamma rhythm and controls sensory responses. Nature 459: 663667.
73. Michaelson SD, Ozkan ED, Aceti M, Maity S, Llamosas N, Weldon M, et al. (2018): SYNGAP1 heterozygosity disrupts sensory processing by reducing touch-related activity within somatosensory cortex circuits. Nat Neurosci 21: 1.
74. Blatow M, Rozov A, Katona I, Hormuzdi SG, Meyer AH, Whittington MA, et al. (2003): A Novel Network of Multipolar Bursting Interneurons Generates Theta Frequency Oscillations in Neocortex. Neuron 38: 805–817. [PubMed: 12797964]
75. Kullmann DM, Lamsa K (2008): Roles of distinct glutamate receptors in induction of anti-Hebbian long-term potentiation. J Physiol 586: 1481–1486. [PubMed: 18187472]
76. McMahon AC, Barnett MW, O'Leary TS, Stoney PN, Collins MO, Papadia S, et al. (2012): SynGAP isoforms exert opposing effects on synaptic strength. Nat Commun 3: 900. [PubMed: 22692543]

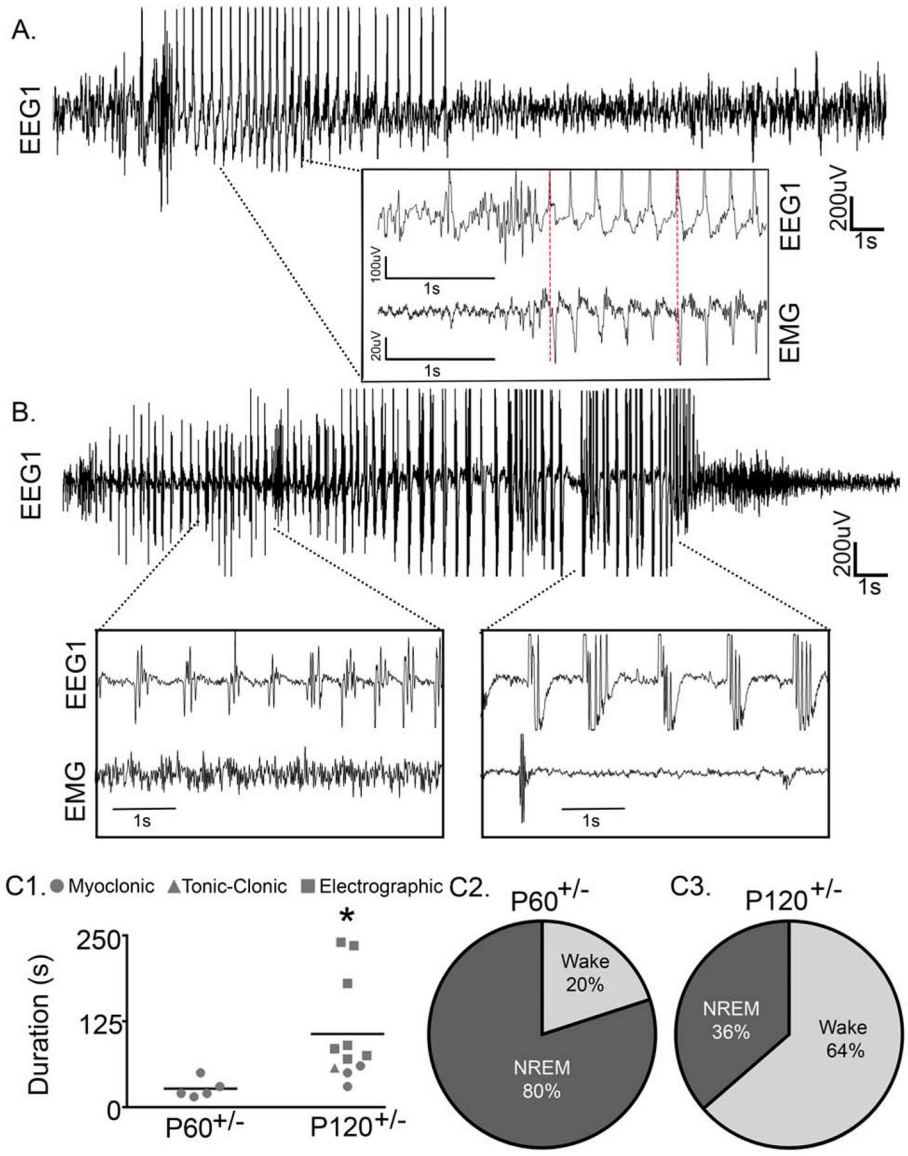

Fig. 1. *Syngap1*$^{+/-}$ mice had recurrent spontaneous seizures.

(A) Representative EEG trace (0.5–50Hz) of a spontaneous myoclonic seizure at P60 during NREM sleep (P60 EEG recordings N=6 *Syngap1*$^{+/-}$ mice). Prototypical time-locked myoclonic jerks were recorded on EMG (see Supplementary Video 1). **(B)** Representative spontaneous tonic-clonic seizure at P120 during NREM sleep (P120 EEG recordings N=7 *Syngap1*$^{+/-}$ mice). **(C1)** Multiple seizure phenotypes emerged at P120, and the average duration of seizures significantly increased from P60 to P120 (*t-test*, t_{14}=2.307, p=0.037). **(C2)** At P60 all seizures were myoclonic and the majority (4/5 seizures; N=2 mice) occurred during NREM. **(C3)** At P120, all myoclonic (3/11 seizures; N=3 mice) and tonic-clonic (1/11 seizures; N=1 mouse) seizures occurred during NREM, whereas all electrographic seizures occurred during wake (7/11 seizures; N=3 mice) (for the electrographic seizure trace see Supplementary Fig. 2). (p<0.05 *, post-hoc Bonferroni).

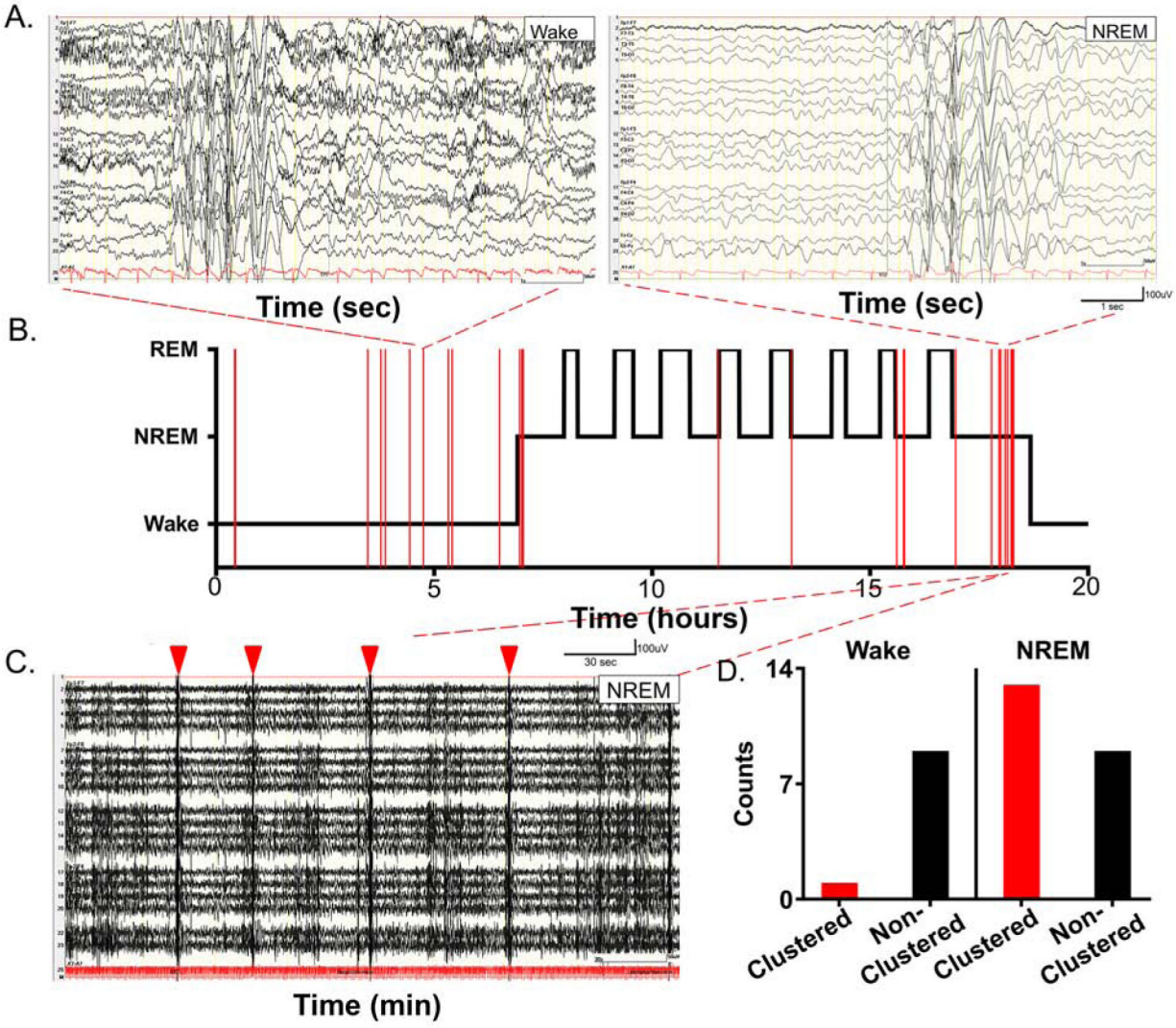

Fig. 2. Ictal events during a 20h overnight EEG recording in a 3-year-old boy with *SYNGAP1* haploinsufficiency.

(A) Identical 3Hz short duration epileptiform events during wake and NREM sleep. **(B)** Hypnogram for the 20h period, with clustering of events identified during NREM sleep. **(C)** 5min EEG trace showed four clustered events (red arrowheads) occurring within a 5min period during the last NREM cycle before wake. Note ictal events occurring at transition points between Wake-NREM and REM-NREM (For a 50min EEG recorded from a 5-year-old girl with *SYNGAP1* haploinsufficiency see Supplemental Fig. 3) **(D)** Bar graphs grouping clustered vs. non-clustered events for Wake and NREM showed affinity for of ictal clustering during NREM (N=1; a 3-year-old-boy with *SYNGAP1* haploinsufficiency). Seizure rates normalized per hour of EEG recording in the raster were Wake=1.27/h; NREM=2.68/h and REM=0/h.

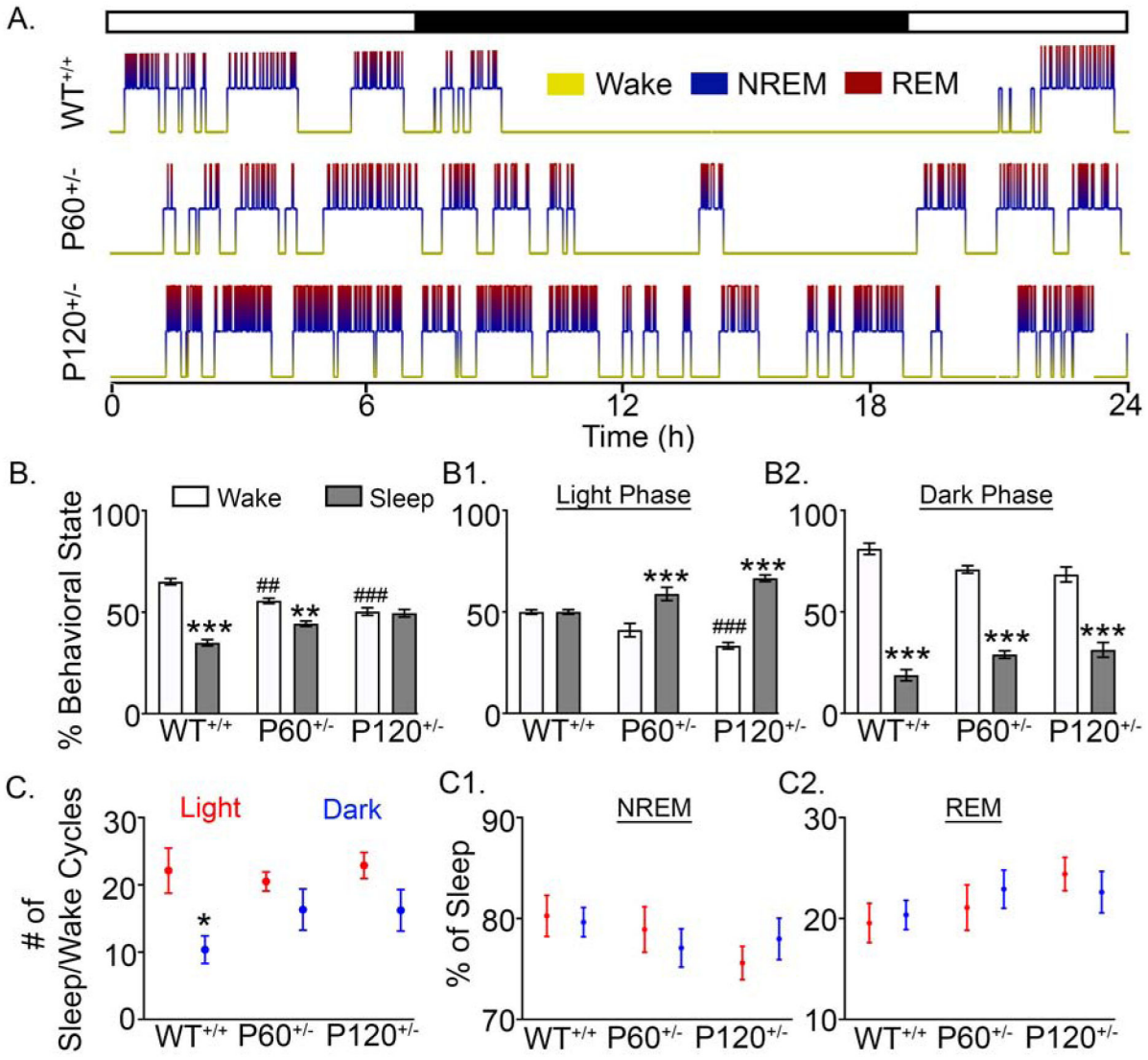

Fig. 3. Progressive alterations in macro-sleep architecture.

(A) 24h hypnograms of nocturnal ultra-radian rhythms in $WT^{+/+}$, $P60^{+/-}$, and $P120^{+/-}$ mice. Regardless of age, all $WT^{+/+}$ mice had consistent macro and micro-sleep architectures (Supplemental Fig. 4). **(B)** $WT^{+/+}$ mice spent significantly less time asleep than awake ($WT^{+/+}$ Wake vs. $WT^{+/+}$ Sleep: 2-way ANOVA, $F_{2,40}$=42.01, p<0.0001). $P60^{+/-}$ mice also spent significantly less time asleep than awake ($P60^{+/-}$ Wake vs. $P60^{+/-}$ Sleep: 2-way ANOVA, $F_{2,40}$=42.01, p=0.002). In contrast, $P120^{+/-}$ mice lacked any significant differences between durations of Wake and Sleep. Between groups, time spent awake significantly decreased in $P60^{+/-}$ ($WT^{+/+}$ Wake vs. $P60^{+/-}$ Wake: 2-way ANOVA, $F_{2,40}$=42.01, p=0.009) and $P120^{+/-}$ mice ($WT^{+/+}$ Wake vs. $P120^{+/-}$ Wake: 2-way ANOVA, $F_{2,40}$=42.01, p<0.0001). **(B1)** During the 12h light phase, in contrast to WT+/+, both $P60^{+/-}$ and $P120^{+/-}$ mice spent more time asleep than awake ($P60^{+/-}$ Light Wake vs. $P60^{+/-}$ Light Sleep: 2-way ANOVA, $F_{2,40}$=40.07, p<0.0001; $P120^{+/-}$ Light Wake vs. $P120^{+/-}$ Light Sleep, p<0.0001). The amount of time $P120^{+/-}$ mice spent awake was significantly lower than $WT^{+/+}$ ($WT^{+/+}$ Light Wake vs. $P120^{+/-}$ Light Wake: $F_{2,40}$=40.0, p<0.0001). **(B2)** $WT^{+/+}$, $P60^{+/-}$, and $P120^{+/-}$ mice all spent

significantly less time asleep than awake during the dark phase ($WT^{+/+}$ Dark Wake vs. $WT^{+/+}$ Dark Sleep: 2-way ANOVA, $F_{2,40}$=9.617, p<0.0001; $P60^{+/-}$ Dark Wake vs. $P60^{+/-}$ Dark Sleep: p<0.0001, $P120^{+/-}$ Dark Wake vs. $P120^{+/-}$ Dark Sleep: p<0.0001). **(C)** Only $WT^{+/+}$ mice had significantly fewer cycles (transitions between sleep and wake) during the dark phase than the light phase ($WT^{+/+}$ Light cycles vs. $WT^{+/+}$ dark cycles: 2-way ANOVA, $F_{2,40}$=0.998, p=0.04. **(C1 & C2)** Although the significant diurnal difference in the number of sleep/wake cycles detected in $WT^{+/+}$ did not occur in $P60^{+/-}$ and $P120^{+/-}$ mice, the microarchitecture of both NREM and REM cycles during sleep was not significantly different. $WT^{+/+}$ N=6 mice, $P60^{+/-}$ N=6 mice, and $P120^{+/-}$ N=7 mice (p<0.05 *, p<0.01 **; p<0.001 ***; p<0.05 #, p<0.01 ##; p<0.001 ###, post-hoc Bonferroni).

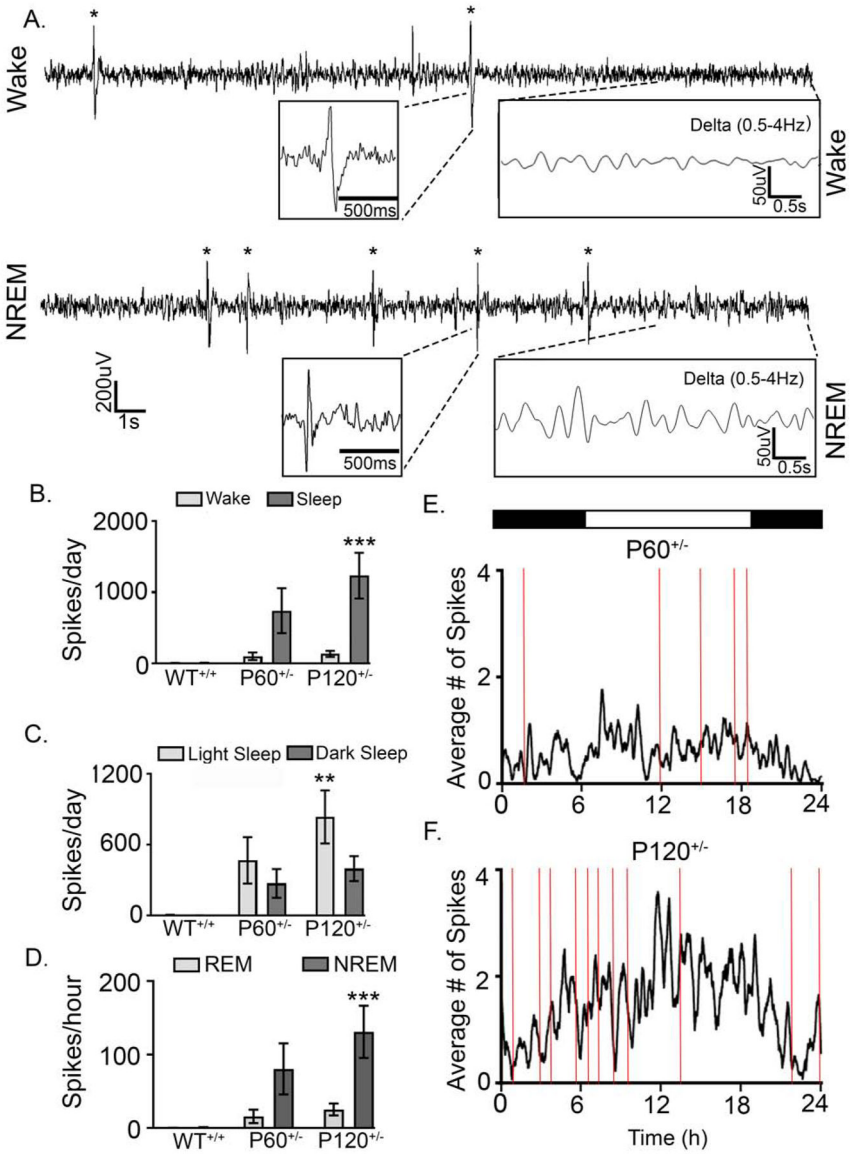

Fig. 4. Progressive interictal spiking during NREM.

(A) 30s EEG trace (0.5–50Hz) during wake of interictal spikes (n=2 spikes; black asterisks) with low amplitude delta power (0.5–4Hz). During NREM sleep, a 30s EEG trace demonstrated interictal spikes (n=5 spikes; black asterisks) with high amplitude delta power (0.5–4Hz). **(B)** Number of spikes during sleep significantly increased in $P120^{+/-}$ compared to WT mice ($WT^{+/+}$ Sleep Spikes vs. $P120^{+/-}$ Sleep Spikes: 2-way ANOVA, $F_{2,\ 40}$=4.80, p=0.0003) **(C)** Number of spikes significantly increased during light sleep in $P120^{+/-}$ mice ($WT^{+/+}$ vs. $P120^{+/}$: 2-way ANOVA, Light Sleep Spikes: $F_{2,40}$=1.33, p=0.0012). **(D)** Interictal spikes significantly increased with age during NREM ($WT^{+/+}$ NREM spikes vs. $P120^{+/-}$ NREM spikes: 2-way ANOVA, $F_{2,\ 40}$=3.508, p=0.0006) **(E & F)** Interictal spikes (black traces) and seizure frequency (red lines) over 24h. $WT^{+/+}$ N=6 mice, $P60^{+/-}$ N=6 mice, and $P120^{+/-}$ N=7 mice (p<0.05 *, p<0.01 **; p<0.001 ***; post-hoc Bonferroni).

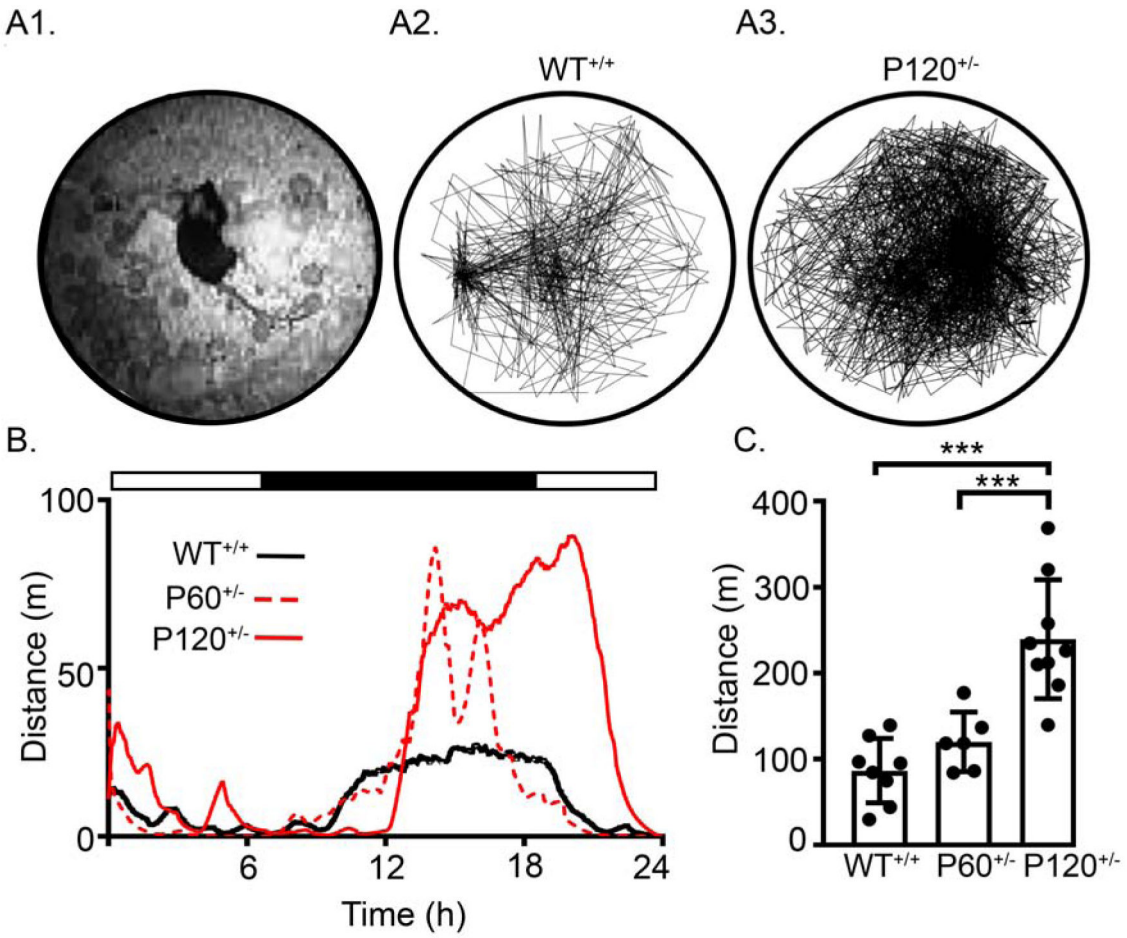

Fig. 5. Progressive increase in activity during 24h recordings.

(A1) Image from the infrared top-view camera utilized for motion tracking. **(A2 & A3)** Representative traces of $WT^{+/+}$ and $P120^{+/-}$ activity over 24h within individual recording chambers. **(B)** A representative local regression for distance traveled over 24h by a $WT^{+/+}$, $P60^{+/-}$, and $P120^{+/-}$ mouse, all mice showed increased activity during the exploration and nesting phase. **(C)** $P120^{+/-}$ mice showed significantly higher activity than $WT^{+/+}$ and $P60^{+/-}$ mice ($WT^{+/+}$ vs. $P120^{+/-}$: 1-Way ANOVA; $F_{2,20}=20.18$, $p<0.001$, $P120^{+/-}$ vs. $P60^{+/-}$: $p<0.001$). $WT^{+/+}$ N=6 mice, $P60^{+/-}$ N=6 mice, and $P120^{+/-}$ N=7 mice. ($p<0.05$ *, $p<0.01$ **; $p<0.001$ ***; post-hoc Bonferroni).

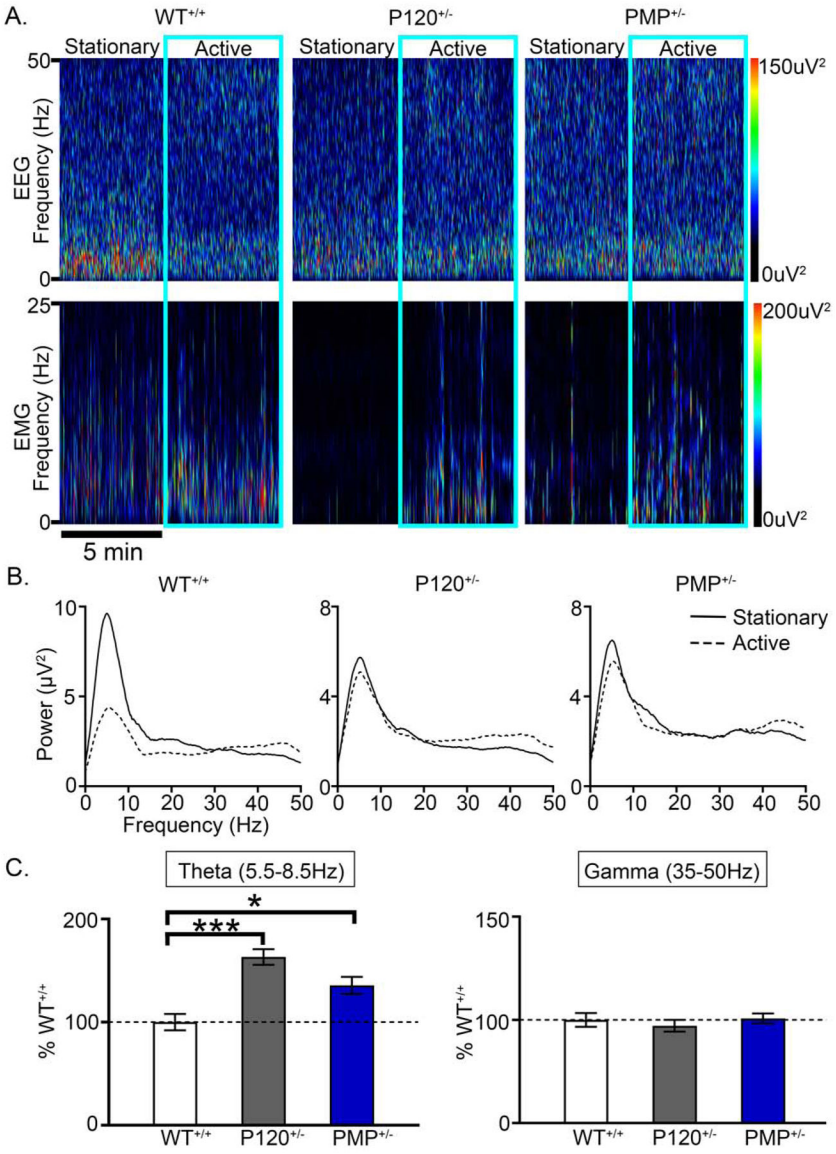

Fig. 6. Progressive impairment of theta power during transitions from inactive to active wake.

(A) EEG and EMG spectral power heat maps of activity-dependent transitions from stationary to active wake in $WT^{+/+}$ mice. $P120^{+/-}$ mice failed to demonstrate an increase in gamma with concurrent decrease in theta. **(B)** Representative spectral frequency traces in $WT^{+/+}$ and P120 $^{+/-}$ mice during stationary to active transitions. **(C)** The lack of theta modulation in $P120^{+/-}$ mice during transitions from inactive to active wake was significant ($WT^{+/+}$ theta vs. $P120^{+/-}$ theta %: 1-way ANOVA, $F_{2,22}$=13.51, p<0.0001). PMP administration (2mg/kg; I.P.) at 10am and 6pm failed to significantly rescue theta modulation with acute dosing ($WT^{+/+}$ theta vs. $PMP^{+/-}$ theta %: 1-way ANOVA, $F_{2,22}$=13.51, p=0.017). During transitions from inactive to active wake, gamma modulation was not significantly impaired. $WT^{+/+}$ N=6 mice, $P60^{+/-}$ N=6 mice, $P120^{+/-}$ N=7 mice, and $PMP^{+/-}$ N=4 mice. (p<0.05 *, p<0.01 **; p<0.001 ***; post-hoc Bonferroni).

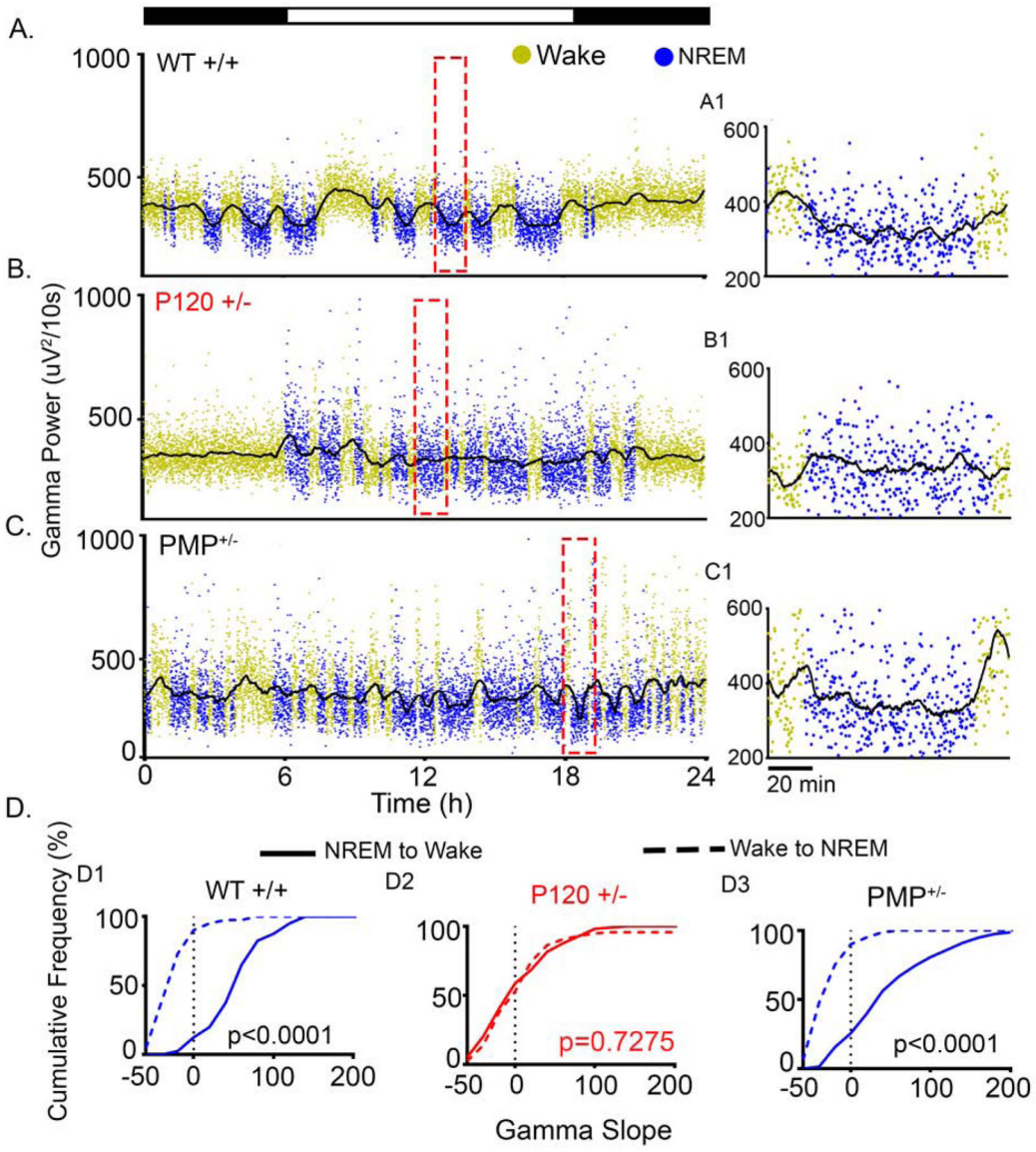

Fig. 7. Gamma during transitions between wake and NREM behavioral state modulation of EEG gamma spectral power.

(A) 24h $WT^{+/+}$ gamma traces had high gamma during wake and low gamma during NREM. **(A1)** Expanded time scales (red boxes in A-C indicate location of expanded timescales in A1–C1) show a gradual fall of gamma from wake to NREM and gradual rise of gamma from NREM to Wake. **(B)** Gamma power in the $P120^{+/-}$ failed to transition to NREM levels, expanded time scale **(B1)** demonstrates the failure of gamma attenuation during a NREM cycle. **(C)** In PMP-administered $P120^{+/-}$ ($PMP^{+/-}$), behavioral-state transitions in gamma power were significantly rescued **(C1)**. **(D)** Cumulative frequency graphs of positive NREM to Wake slopes and negative wake to NREM slopes in $WT^{+/+}$. **(D1)** These slopes were significantly different (*t-test*, t_{275}=10.59, p<0.001) between the two independent transition states. **(D2)** No behavioral-state dependent modulation of gamma power occurred in $P120^{+/-}$ (*t-test*, t_{327}=0.3488, p=0.7275). **(D3)** PMP administration restored gamma power behavioral-

state dependent modulation (*t-test*, t_{156}= 9.854, p<0.0001). $WT^{+/+}$ N=6 mice, $P60^{+/-}$ N=6 mice, $P120^{+/-}$ N=7 mice, and $PMP^{+/-}$ N=4 mice.

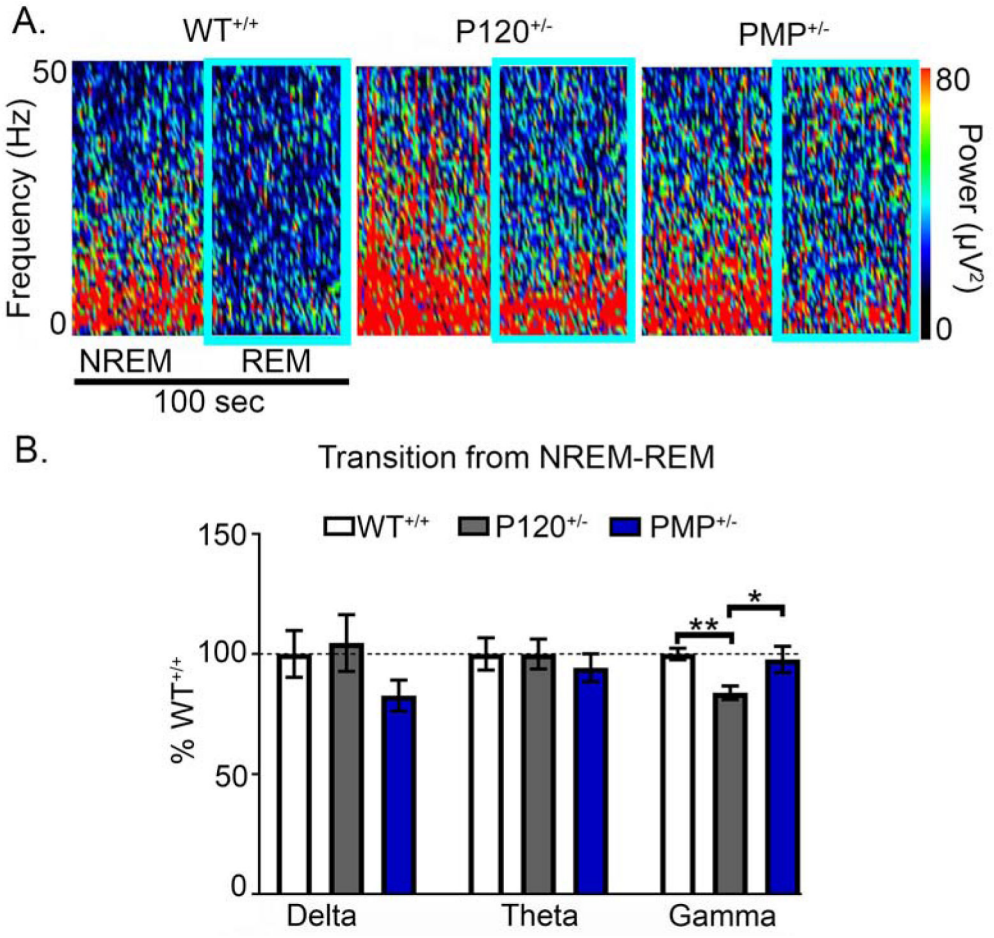

Fig. 8. PMP rescued gamma modulation during transitions from NREM to REM.

(A) Spectral power heat maps during NREM to REM transitions in $WT^{+/+}$, $P120^{+/-}$, and $PMP^{+/-}$ mice. **(B)** A significant decrease in gamma power during NREM to REM transitions was demonstrated in $P120^{+/-}$ mice ($WT^{+/+}$ Gamma vs. $P120^{+/-}$ Gamma % 1-way ANOVA, $F_{2,105}$=6.11, p=0.005), but was significantly rescued by PMP administration ($P120^{+/-}$ Gamma vs. PMP Gamma: 1-way ANOVA, $F_{2,105}$ = 6.11, p=0.026. $WT^{+/+}$ N=6 mice, $P60^{+/-}$ N=6 mice, $P120^{+/-}$ N=7 mice, and $PMP^{+/-}$ N=4 mice. (p<0.05 * and p<0.01 **; post-hoc Bonferroni).

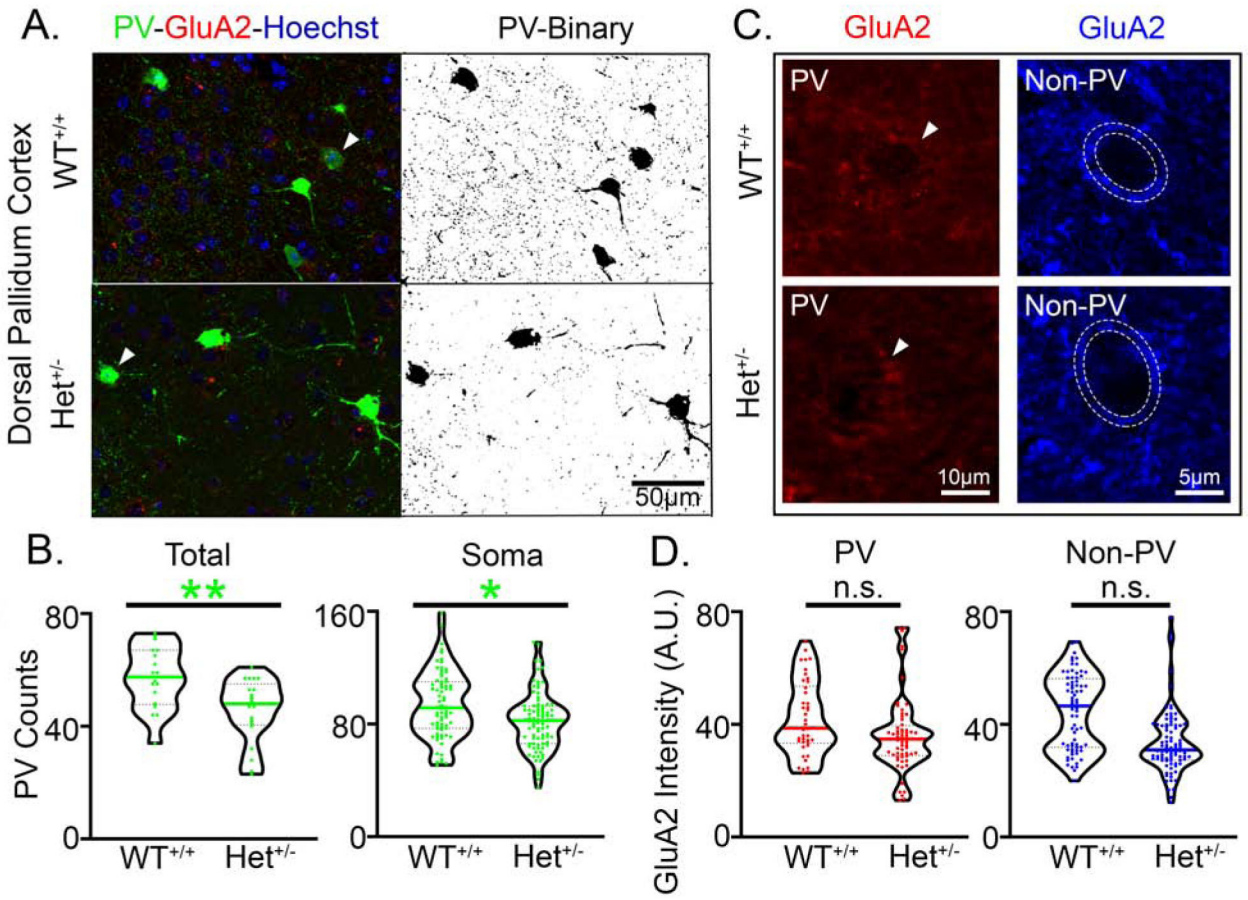

Fig. 9. PV+IN deficits in pre-frontal cortex.

(A) Representative 40X Z-Stack image from the dorsal pallidum (DP) cortex in $WT^{+/+}$ and *Syngap1*$^{+/-}$ mice ($Het^{+/-}$) mice (white arrowheads indicate PV+INs shown in **C**). **(B)** PV immunofluorescence represented by total PV+ puncta in the 40X image showed a significantly lower putative presynaptic puncta in the $Het^{+/-}$ mice (*Nested t-test*, t_{37}=3.24, p=0.0026). PV+ puncta counts onto non-PV somas were also significantly lower (*Nested t-test*, t_{14}=2.398, p=0.03). **(C)** Representative images of GluA2 fluorescence on PV (red) and non-PV (blue) somas in the DP cortex in $WT^{+/+}$ and $Het^{+/-}$ mice (white arrowheads indicate soma of respective PV+INs from **A**). **(D)** There were no significant differences in GluA2 expression on PV+IN (*Nested t-test*, t_{14}=1.230, p=0.2391) or non-PV (*Nested t-test*, t_{14}=1.883, p=0.0806) neurons in the DP cortex. N=8 *Syngap1*$^{+/-}$ mice and N=8 $WT^{+/+}$ mice (p<0.05 *, p<0.01 **).

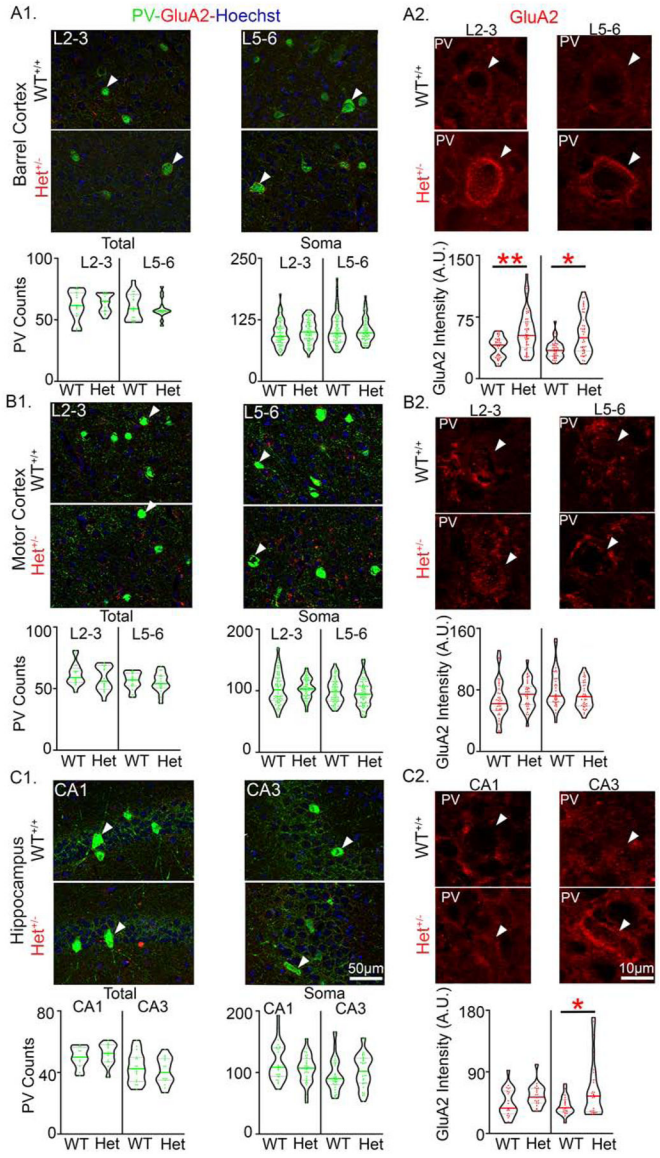

Fig. 10. Increased GluA2 expression on PV+IN soma were region specific

(A1) Representative 40X Z-stack images of $WT^{+/+}$ and *Syngap1*$^{+/-}$ mice ($Het^{+/-}$) from barrel cortex (BCX) layers 2–3 and 5–6 (L2–3 and L5–6). White arrowheads indicate PV +INs shown in A2 for BCX L2–3 and L5–6, respectively. Total PV+ puncta counts and somatic PV+ puncta counts on non-PV soma were not significantly different in the BCX. **(A2)** Representative Z-stack images of GluA2 immunofluorescence on PV+INs in L2–3 and L5–6. $Het^{+/-}$ GluA2 expression was significantly higher on PV+INs in both BCX L2–3 (*Nested t-test*, t_{12}=3.467 p=0.0047) and L5–6 (*Nested t-test*, t_{12}=2.361, p=0.036). White arrowheads indicate soma of respective PV+INs from **A1**. **(B1)** Representative 40X Z-stack images from motor cortex (MCX) L2–3 and L5–6. Total PV+ puncta counts and somatic PV + puncta counts on non-PV soma were not significantly different in the MCX. White arrow heads indicate PV+INs shown in B2 for MCX L2–3 and L5–6, respectively. **(B2)** Representative Z-stack images of GluA2 expression was not significantly different for PV

+INs in the MCX L2/3 and L5/6. White arrowheads indicate soma of respective PV+INs from **B1**. **(C1)** Representative 40X Z-stack images from hippocampal CA1 and CA3. White arrow heads indicate PV+INs show in C2 for CA1 and CA3, respectively. Total PV+ puncta counts and somatic PV+ puncta counts on non-PV soma were not significantly different in CA1 or CA3. **(C2)** Representative images of GluA2 immunofluorescence on PV+INs. CA3 $Het^{+/-}$ PV+INs had a significant increase in GluA2 expression (*Nested t-test*, t_{12}=2.331, p=0.038). White arrowheads indicate soma of respective PV+INs from **C1**. N=8 *Syngap1*$^{+/-}$ mice and N=8 $WT^{+/+}$ mice (p<0.05 *, p<0.01 **).